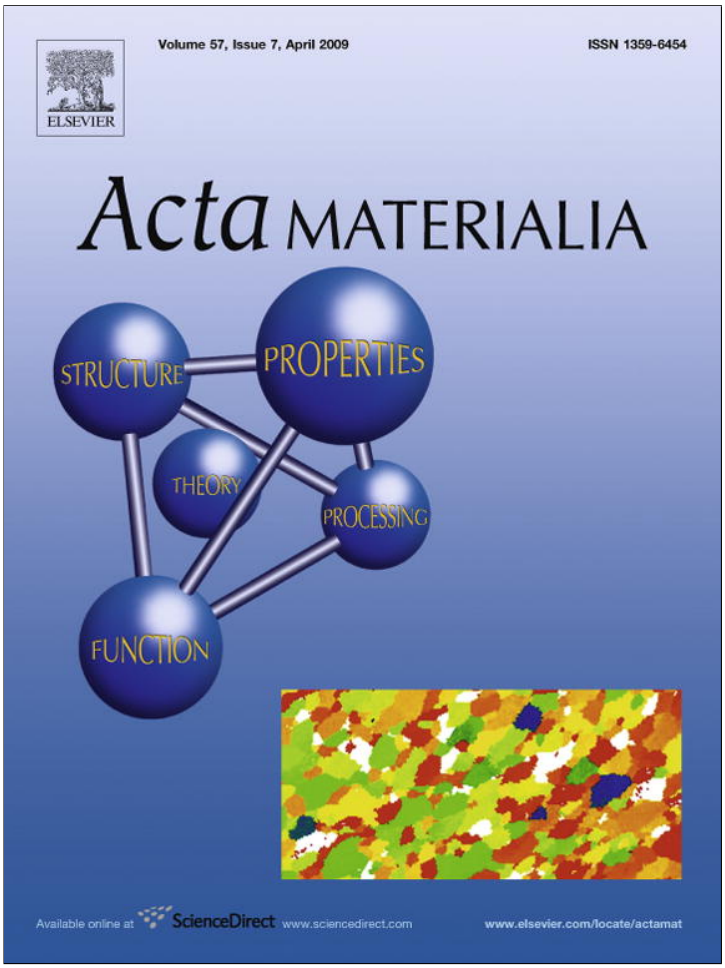

Available online at www.sciencedirect.com
ScienceDirect
Acta Materialia 57 (2009) 2217–2228
Acta MATERIALIA
www.elsevier.com/locate/actamat

Enhanced ductility of nanomaterials through optimization of grain boundary sliding and diffusion processes

I.A. Ovid'ko, A.G. Sheinerman *

Institute for Problems of Mechanical Engineering, Russian Academy of Sciences, Bolshoj 61, Vas. Ostrov, St. Petersburg 199178, Russia

Received 24 April 2008; received in revised form 5 January 2009; accepted 22 January 2009
Available online 2 March 2009

Abstract

A theoretical model is suggested which describes the combined effects of grain boundary (GB) sliding and diffusion on strain hardening and ductility of nanocrystalline materials (NCMs). Within the model, GB sliding creates disclination dipoles near triple junctions, inducing high elastic stresses and resulting in pronounced strain hardening. At the same time, GB diffusion partly relieves disclination stresses, thereby decreasing strain hardening. It is theoretically shown that good ductility of NCMs can be reached due to optimization of GB sliding and diffusion processes providing optimum strain hardening. The latter suppresses plastic strain instability and thus enhances tensile ductility. At the same time, with the optimum strain hardening, the applied stresses reach their critical level at which NCMs fracture only if overall plastic strain is sufficiently large.

Keywords: Nanocrystalline materials; Plastic deformation; Ductility; Grain boundary diffusion

1. Introduction

Nanocrystalline metals and ceramics showing superior strength and hardness are excellent candidates for a variety of new industrial applications (e.g. [1–7]). The key factor limiting the practical use of nanocrystalline materials (NCMs) is the low tensile ductility that most exhibit. At the same time, several research groups have reported good ductility or even superplasticity of NCMs fabricated and processed at certain conditions [8–13]. The fundamental reasons for the very different plastic behaviors (low ductility shown by most NCMs and good/high ductility shown by certain NCMs) are not understood. In any event, the mechanical characteristics of nanocrystalline metals and ceramics crucially depend on specific deformation mechanisms operating in these materials [1–7], and the ductility of NCMs should be adequately described in terms of the deformation mechanisms. Among the specific deformation mechanisms, grain boundary (GB) sliding is believed to be crucially important in NCMs in certain situations. In particular, GB sliding and associated diffusion processes have been shown experimentally to play a dominant role in superplastic deformation of nanocrystalline and ultrafine-grained materials [7,8,14,15]. Also, GB sliding and GB diffusional creep (Coble creep) effectively operate in NCMs in conventional deformation regimes at low stresses and strain rates [6,16]. Computer simulations [17–20] have highlighted the role of GB sliding as one of the key mechanisms of plastic deformation in NCMs, especially at very high stresses and strain rates (see also review in Ref. [2] and references therein). Following Refs. [17,20], GB sliding in NCMs with the finest grains creates stresses that are accommodated by movement of GBs and their triple junctions. In addition, recent computer simulations [21] demonstrated that GB sliding along with GB diffusion provides the main contribution to plastic deformation of nanocrystalline Cu with a grain size of 30 nm at room temperature. Recently, several theoretical models [22–29] have been proposed focusing on the role of GB sliding and diffusion in plastic flow and fracture processes in NCMs. Given the

* Corresponding author.
E-mail addresses: ovidko@def.ipme.ru (I.A. Ovid'ko), shein77@mail.ru (A.G. Sheinerman).

1359-6454/$36.00 © 2009 Acta Materialia Inc. Published by Elsevier Ltd. All rights reserved.
doi:10.1016/j.actamat.2009.01.030

above results from experiments, computer simulations and theoretical models, there is much interest in understanding the effects of GB sliding and diffusion processes on the tensile ductility of NCMs. The main aims of this paper are to suggest a theoretical model describing these combined effects and, with the results of the model, to reveal the conditions at which NCMs show enhanced ductility due to optimization of the effects of GB sliding and diffusion processes.

2. Effects of grain boundary sliding and diffusion processes on tensile ductility of nanomaterials: general aspects

In general, one can distinguish the following three basic factors that diminish the tensile ductility of NCMs: (i) fabrication-produced flaws; (ii) early fracture associated with crack nucleation and growth instability; and (iii) plastic strain instability associated with catastrophic shear banding and necking [30,31]. In recent years, significant progress has been reached in fabrication of artifact-free NCMs, in particular those characterized by both superior strength and good ductility (e.g. [8,10–12,15,32–35]). In these materials, there are no fabrication-produced flaws, and the instabilities (ii) and (iii) are suppressed. In general, suppression of shear banding can be achieved through enhancement of strain hardening and/or strain rate sensitivity [7,30–32], while crack nucleation is suppressed if dangerous stress sources (defects creating high local stresses) are not generated during plastic deformation. The fulfilment of these conditions serves as the selection rule for plastic flow mechanisms responsible for enhanced ductility of NCMs.

We think that the combined effects of GB sliding and diffusion, if these are optimized, are capable of suppressing both catastrophic shear banding and nucleation and growth of cracks in artifact-free NCMs. GB sliding in NCMs causes the strain hardening that suppresses plastic strain instability associated with catastrophic shear banding and necking. More precisely, GB sliding through triple junctions of GBs produces defects at and near these junctions [23–25,29,36]. The GB-sliding-produced defects are GB dislocations (associated with deformation incompatibilities) [23–25] and dipoles of wedge disclinations (rotational defects associated with crystal lattice orientation incompatibilities) [29,36]. Fig. 1 schematically shows the formation of wedge disclination dipoles due to GB sliding in NCMs; for more details, see Refs. [29,36]. (Also, a similar process of formation of disclinations occurs due to stress-driven migration of GBs in NCMs [37].) Following Ref. [29], wedge disclination dipoles appearing in NCMs during GB sliding create very pronounced strain hardening. In this case, the rate of strain hardening is much higher than the rate of strain hardening [24] due to the dislocation storage at triple junctions due to GB sliding in NCMs. The calculated strain hardening [29] appeared to be so high that it leads to values similar to those obtained experimentally for the ultimate stress at very small plastic strains (1–2% for Ni and less than 1% for Cu). Therefore, one can assume

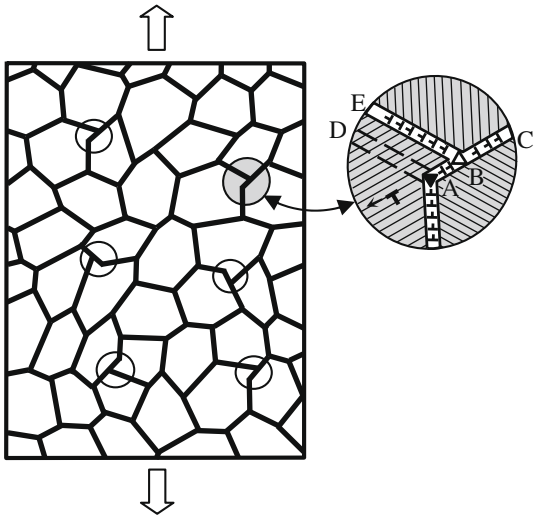

Fig. 1. Nanocrystalline specimen under tensile plastic deformation. Magnified inset highlights formation of wedge disclination dipoles due to GB sliding. In this inset, GB AD moves to another position BE, which leads to the formation of opposite-sign disclinations in points A and B. GB sliding is accommodated by emission of lattice dislocations from triple junction A.

that the dramatic strain hardening created by GB sliding [29], although suppressing plastic strain instability due to necking, commonly induces early fracture associated with intensive formation and growth of cracks.

Nevertheless, experimentally detected examples of substantial tensile ductility [8,10–12,15,32–35] of NCMs are naturally attributed to the strain hardening caused by GB sliding, if it is relieved by some accommodation mechanisms. In particular, GB diffusion can significantly decrease or even completely remove the disclination stresses and the associated strain hardening in NCMs. For instance, the role of diffusion processes is significant in deformation regimes at high temperatures and/or low strain rates, and relaxation of the disclination stresses can effectively occur by diffusion processes. We think these processes are capable of suppressing crack nucleation and growth, resulting in good ductility of NCMs under certain conditions. The quantitative analysis of these conditions will be performed in the following sections.

Our further analysis is focused on suppression of plastic strain instabilities through pronounced strain hardening in NCMs, taking into account strain rate effects. It is important to note that our key assumption that GB sliding and diffusion play the dominant role in plastic deformation in NCMs at certain conditions is in agreement with several experiments concerning strain rate sensitivity of such materials. Let us briefly discuss this subject. The strain rate sensitivity is commonly defined as (e.g. [32]) $m = (\partial \ln \sigma / \partial \ln \dot{\varepsilon})_{\varepsilon,T}$, where ε denotes the plastic strain degree, $\dot{\varepsilon}$ the plastic strain rate, and T the temperature. If the strain rate sensitivity m of a material is positive and sufficiently large, neck formation is suppressed. (For instance, superplasticity is specified by m being around 0.3 or larger; e.g. [38].) This

is because a local increase in the plastic strain rate in a nucleus of the neck region leads to a local increase in the flow stress. The values of $m = 0.5$ and $m = 1$ generally characterize plastic deformation by GB sliding and Coble creep, respectively (e.g. [38,39]). Experimental results with $m < 0.2$ are attributed to some form of lattice dislocation slip.

In general, experiments with NCMs show that the values of their strain rate sensitivity m are in a wide range, even for materials with the same chemical composition. This variety in m can be attributed to its sensitivity to many structural characteristics (mean grain size, grain size distribution, absence/presence of fabrication-produced flaws, typical structures of grain boundaries), which, in general, are different in NCMs produced by different fabrication techniques. For instance, there are experimental data showing that the value of m in nanocrystalline metals (Cu, Ni) and ceramics (ZnO, TiO_2) is on the order of 0.1 or lower [32,40–44]. At the same time, there are several examples of NCMs exhibiting $m > 0.2$. In particular, high values of strain rate sensitivity m have been found experimentally in nanocrystalline Cu at room temperature. For instance, Jiang et al. [45] found that in room temperature creep tests of nanocrystalline Cu, m takes the values of 0.243 and 1 at stress levels of $\sigma > 175$ MPa and $\sigma < 175$ MPa, respectively. Lu et al. [46] reported the experimental value of $m \approx 1$ in the course of superplastic deformation of nanocrystalline Cu at room temperature. Wang et al. [47] experimentally studied nanocrystalline Ni in room temperature creep tests and found $m \approx 0.85$, 0.5 and 0.2 in nanocrystalline specimens with mean grain sizes $d = 6$, 20 and 40 nm, respectively. Yin et al. [48] reported $m \approx 1$ and 0.18 for nanocrystalline Ni with mean grain sizes $d = 30$ nm tested at room temperature and 373 K, respectively. Furthermore, Wang et al. [49] experimentally documented the strain rate sensitivity $m \approx 0.5$ in the superplastic deformation regime of nanocrystalline Ni–Co alloy at a temperature of 773 K. Values of $m \approx 0.5$ and 1 were found in experiments [15] focused on nanocrystalline Si_3N_4 ceramics showing superplastic deformation in compression over a wide range of strain rates and temperatures. Superplasticity of zirconia–alumina–spinel nanoceramic composites characterized by $m \approx 0.5$ was experimentally observed by Zhou et al. [50]. In the light of the experimental works discussed above, our assumption that GB sliding and diffusion play the dominant role in plastic deformation of nanocrystalline materials under certain conditions (low strain rates, high or moderate temperatures) is in good agreement with several experiments on the strain rate sensitivity of such materials.

3. Effect of disclinations on strain hardening in the absence of grain boundary diffusion

Let us estimate the effect of disclinations on strain hardening in NCMs. To do so, we consider a nanocrystalline solid, deformed mostly by GB sliding, under a uniaxial tensile load (Fig. 1). In a first approximation, we assume that essential GB sliding is carried only by favorably oriented GBs the planes of which make small angles with the directions of the maximum shear stress (which, in turn, make an angle $\pi/4$ with the loading direction). Following Orowan [51], the plastic shear strain is defined as the average sliding distance divided by average distance between the sliding planes. In this case, GB sliding is characterized by the macroscopic plastic shear strain (acting in the planes making an angle $\pi/4$ with the loading direction) $\varepsilon \approx \alpha p/d$, where d is the mean grain size, p is the mean value of the triple junction translation produced by GB sliding, and α (<1) is the fraction of GBs that carry GB sliding. Note that, according to this definition, the plastic tensile strain along the loading direction is equal to ε.

In this section, we examine tensile deformation of NCMs at low temperatures, in which case the effects of diffusion can be neglected. Let us estimate the energy change ΔW_0 of the nanocrystalline specimen due to GB sliding that creates disclination dipoles. (Hereinafter the subscript "0" specifies the absence of GB diffusion.) In a first approximation, the energy change ΔW_0 (per disclination dipole and per unit disclination length) can be estimated as [29]:

$$\Delta W_0 = W_0^{dip} + (\tau_f - \tau)p, \tag{1}$$

where W_0^{dip} is the self-energy of the disclination array (per disclination dipole), the term $(\tau_f - \tau)p$ characterizes the opposite of the work of the shear stress τ spent to GB sliding, and τ_f is the internal stress that characterizes resistance to GB sliding along plane GBs (in the absence of the disclination dipoles).

Eq. (1) takes into account the fact that disclination dipoles do not interact with the shear stress τ. The self-energy W_0^{dip} of the disclination array can be roughly estimated as the sum of the self-energies of individual disclination dipoles. The interaction between different disclination dipoles leads to the mutual screening of their stress fields. This effect is accounted for in a first approximation by assigning a screening length R to the stresses of the disclination dipoles. Thus, the energy W_0^{dip} can be considered as the mean energy of disclination dipoles (per unit disclination length) whose stress fields are screened at some screening length due to the dipole–dipole interaction. In the standard approximation that a nanocrystalline specimen is an elastically isotropic solid with the shear modulus G and Poisson's ratio ν, the characteristic energy W_0^{dip} is estimated as [52]

$$W_0^{dip} = \frac{A\omega^2 p^2}{2}\left\{\ln\frac{R}{p} + \frac{3}{2}\right\}, \tag{2}$$

where ω is the mean absolute value of the disclination strength, and $A = G/[2\pi(1-\nu)]$.

Plastic flow is energetically favorable if $\partial\Delta W_0/\partial p < 0$, and unfavorable otherwise. In the case of a quasi-equilibrium plastic deformation, we have: $\partial\Delta W_0/\partial p = 0$. With Eqs. (1) and (2) and the expression $p = \varepsilon d/\alpha$, the latter

equality yields the following expression for the disclination-induced contribution τ_d to the total flow stress:[1] $\tau = \tau_f + \tau_{d0}$, where

$$\tau_{d0} = \frac{A\omega^2\varepsilon}{\alpha}\left(\ln\frac{\alpha R}{\varepsilon d} + 1\right). \quad (3)$$

According to Eq. (3), τ_{d0} increases with rising ε, if $\varepsilon < \alpha R/d$. Eq. (3) describes strain hardening due to the formation of GB disclinations. This hardening is inherent to NCMs where the amounts of GBs and their triple junctions are very large, in contrast to coarse-grained polycrystals characterized by low amounts of GBs and their triple junctions.

Let us estimate the characteristic values of τ_{d0}, for nanocrystalline Cu (having a shear modulus $G = 46$ GPa and Poisson's ratio $\nu = 0.35$ [53]), Ni ($G = 73$ GPa and $\nu = 0.31$ [53]) and $\alpha - Al_2O_3$ (corundum) ($G = 169$ GPa and $\nu = 0.23$ [54]). In the following, one should take into account that, for uniaxial tensile load, we have: $\tau = \sigma_t/2$, where σ_t is the applied load. Similarly, the quantity τ_f can be interpreted as half of the tensile yield stress σ_y specifying the start of plastic flow carried by GB sliding: $\tau_f = \sigma_y/2$. For definiteness, the characteristics of the defect configuration under consideration are taken as follows: $R = 3d, \alpha = 1/3$, and $\omega = \pi/9 (= 20^\circ)$. With these characteristics and Eq. (3), in the case of nanocrystalline Cu, we obtain: $\tau_{d0} \approx 0.23$ GPa at $\varepsilon = 0.01$. For Ni, we find: $\tau_{d0} \approx 0.35$ and 0.61 GPa at $\varepsilon = 0.01$ and 0.02, respectively. With the same characteristics, in the case of nanocrystalline $\alpha - Al_2O_3$, Eq. (3) yields: $\tau_{d0} \approx 0.72$ and 1.25 GPa at $\varepsilon = 0.01$ and 0.02, respectively.

From the above estimates it follows that even for low plastic strain, the formation of GB disclinations causes dramatic strain hardening in NCMs and can thereby suppress plastic strain instability. At the same time, disclinations create in their vicinity extremely large stresses, which can initiate the generation of cracks [29] and eventually result in the complete fracture of the material. This view is in good agreement with the results of our theoretical analysis, because, according to Eq. (3), the stress τ_{d0} is so large that the value of σ_t ($\sigma_t = \sigma_y + 2\tau_{d0}$) reaches the experimental ultimate tensile strength σ_B of the examined materials at very small strain ε. For example, for Ni with a grain size of 44 nm, we have $\sigma_y \approx 0.5$ GPa and $\sigma_B \approx 1.1$ GPa [55], whereas for Ni–15%Fe with a grain size of 9 nm, one obtains $\sigma_y \approx 1.2$ GPa and $\sigma_B \approx 2.3$ GPa [55]. The above values of the ultimate stress σ_B for Ni and Ni–15%Fe are reached at strains ε as small as 0.01 and 0.02, respectively.

However, at sufficiently high temperatures and/or low enough strain rates, high disclination stresses can be relaxed by intensive GB diffusion. In this case, disclination formation causes moderate strain hardening that can suppress plastic strain instability but, at the same time, does not initiate formation and growth of crack (see next section).

[1] A similar expression for τ_{d0} has been derived in Ref. [29]. But in the expression obtained in Ref. [29], the term "+1" has been erroneously omitted. Here we correct this error.

4. Effects of grain boundary diffusion on disclination-induced strain hardening

Let us consider the effects of diffusion on the disclination-induced strengthening. In the situation with high enough temperatures and/or sufficiently low strain rates, diffusion is rather intensive. In the situation discussed, diffusion partly relieves the stresses created by disclination dipoles and thus reduces their strain energies. This accommodating effect of diffusion results in a reduction in the applied stress necessary to provide GB sliding accompanied by the formation of disclination dipoles.

To elucidate the effects of diffusion on strain hardening and to estimate the applied stress τ (as a function of plastic strain, strain rate, temperature and material parameters) needed for GB sliding in the presence of GB diffusion, we will use the following model assumptions. First, we suppose that GB diffusion is the dominant accommodation mechanism for the stresses of disclination dipoles. In particular, GB diffusion causes an accommodating effect larger than that produced by bulk diffusion. Second, we consider diffusion processes occurring along a straight, infinite model GB. Next, we suppose that GB sliding leads to the formation of disclination dipoles whose contribution to strain hardening is large compared to the effects [24,56–59] attributed to deformation incompatibilities in triple junctions occurring during GB sliding. Finally, we assume that the mean distance between the dipoles (around d/α) is much larger than the mean distance p between the disclinations comprising a dipole, or, in other words, the mean dipole arm. Their effects on each other can then be accounted for by assigning a screening length R to the disclination dipole stresses. In this case, to calculate the effects of diffusion on strain hardening, it is sufficient to consider an individual disclination dipole and calculate its self-energy taking into account GB diffusion.

The stress field of a disclination dipole induces a gradient of chemical potential at the GB, which creates a flux of atoms along the GB. Following Refs. [25,60], atomic diffusion along a GB is realized via a change in its thickness (see Fig. 2a and b). In turn, the change in the GB thickness creates elastic displacements, strains and stresses in adjacent grains. Therefore, the elastic fields of the disclination dipole are affected by GB diffusion, which tends to relieve these elastic fields.

(Generally speaking, the assumption [25,60] that the atomic diffusion along a GB is realized via a change in its thickness represents a simplified view on the problem. It is true that the additional atoms will create additional stresses and strains, but diffusion might not come only from the changes in GB thickness. In particular, there is a flow of atoms from a GB region into grain interior regions in its

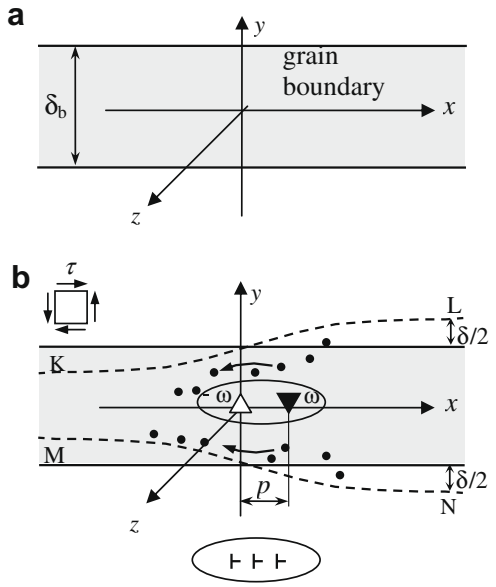

Fig. 2. Flat infinite GB in a bicrystal. (a) Disclination-free GB. (b) GB contains a disclination dipole whose stresses induce GB diffusion and create elastic strains of adjacent grains. The ellipses show equivalency between the disclination dipole examined and a continuous distribution of edge dislocations. The region bounded by dashed curves KL and MN represents a virtual GB in the imaginary situation where the presence of extra atoms or deficit in atoms due to both the presence of the disclination dipole and diffusion is described as the change $\delta(x,t)$ in GB thickness compared to its disclination-free state. Time evolution of the change $(\delta(x,t))$ in GB thickness is used in description of diffusion-conducted evolution of the stresses/strains within the GB and in its vicinity (for details, see text).

vicinity and a reverse flow. Thus, additional atoms are present and diffuse in both GB and grain interior regions. Nevertheless, for simplicity, it is convenient and effective to formally exploit the approach [25,60] based on the change in the GB thickness as the key parameter that describes evolution of the diffusing atoms within the GB area and its vicinity. That is, though the approach [25,60] uses a simplified view ("diffusion along a GB is realized via a change in its thickness"), it captures the essential physics of the problem that we are studying here.)

To calculate the self-energy of a disclination dipole in the presence of GB diffusion, consider a straight, infinite GB (Fig. 2b) serving as a model of real nanoscale GBs. At the initial time $t = 0$ under the action of an applied shear stress τ the upper grain starts to slide relative to the bottom one. As a result, according to Refs. [29,36], an isolated dipole of wedge disclinations with strengths ω and $-\omega$ and dipole arm p forms at the GB. Let us introduce a Cartesian coordinate system (x,y,z) as shown in Fig. 2. We also denote the thickness of the disclination-free GB as δ_b. The left dipole disclination $-\omega$ is located at the point $x = 0$, while the position $x = p$ of the right disclination moves due to GB sliding. The position $x = p$ of the right disclination can be related to the shear strain rate $\dot{\varepsilon}$ (which is assumed to be constant) and deformation time t as $p = \gamma t$, where $\gamma = \dot{\varepsilon} d/\alpha$.

Under these assumptions, we have calculated the strain energy of the disclination dipole (see Appendix). In the case where the dipole arm p and characteristic diffusion length (defined below) are small compared to the dipole screening length R, the dipole strain energy W^{dip} per unit disclination length has been found as follows:

$$W^{dip}(R \gg (p,(\lambda t)^{1/3})) = \frac{A\omega^2 p^2}{2}\left[\ln\frac{R}{p} + \frac{3}{2} - f(s)\right]. \quad (4)$$

Here $\lambda = (1+\nu)GD_b\delta_b\Omega/[3(1-\nu)k_BT]$, D_b denotes the GB diffusion coefficient, Ω is the atomic volume, k_B is the Boltzmann constant, T is the absolute temperature, $s = \lambda t/p^3$ is the cube of the ratio of the characteristic diffusion length $(\lambda t)^{1/3}$ to the dipole arm p, and

$$f(u) = \int_0^\infty \left(\frac{2(1-\cos k)}{k^3} - \frac{1 - 2\cos k\exp(-uk^3) + \exp(-2uk^3)}{k^3(u^2k^4+1)}\right)dk. \quad (5)$$

The first two terms in brackets in Eq. (4) give the self-energy of the disclination dipole in the absence of GB diffusion, while the third term accounts for the negative contribution of GB diffusion to the disclination dipole energy. For $s = 0$, when GB diffusion is absent, we have $f(s=0) = 0$. At the same time, in the case of intense diffusion $(s \gtrsim 1)$, we obtain the following simple asymptotic expression for $f(s)$:

$$f(s \gtrsim 1) \approx \frac{1}{3}\ln s + 1.08. \quad (6)$$

For illustration, the dependence $f(s)$ and its asymptote at large s, $y = (1/3)\ln s + 1.08$, are shown in Fig. 3 as solid and dashed curves, respectively.

Thus, we have found the expression for the energy of a disclination dipole in the presence of GB diffusion. Now the energy ΔW (per disclination dipole and per unit disclination length) associated with GB sliding in the presence of GB diffusion is calculated in the same way as the energy ΔW_0 (see Eq. (1)):

$$\Delta W = W^{dip} + (\tau_f - \tau)p. \quad (7)$$

For convenience, we relate the screening length R appearing in Eq. (4) to the grain size d. Since the screening of the elastic fields of the disclination dipoles is supposed to be realized by the disclination dipoles originating in the

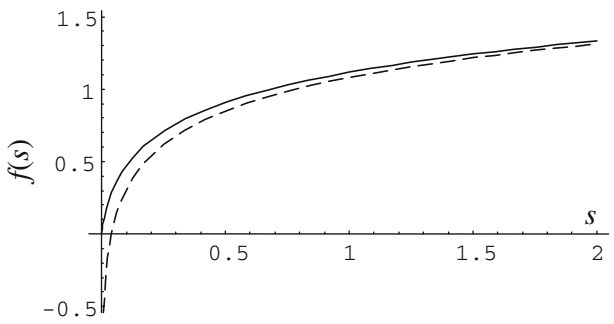

Fig. 3. Dependence $f(s)$ (solid curve) and its asymptote at $s \to \infty, y = (1/3)\ln s + 1.08$ (dashed curve).

neighboring triple junctions, as a first approximation, we put $R = \kappa d$, where κ is a factor ranging from 1 to 10. Then substitution of Eqs. (4) and (7) into the relation $\partial \Delta W/\partial p = 0$ gives the following relation for the stress $\tau : \tau = \tau_f + \tau_d$, where

$$\tau_d = \frac{A\omega^2\varepsilon}{\alpha}\left[\ln\frac{\kappa\alpha}{\varepsilon} + 1 - f(s) + sf'(s)\right]. \quad (8)$$

It is important to note that Eq. (8) is valid for values of deformation time t and temperature T that are not too large; under these conditions the characteristic diffusion length $(\lambda t)^{1/3}$ is smaller than the screening length R. When the diffusion length $(\lambda t)^{1/3}$ becomes larger than, or close to, the screening length R, diffusion eliminates most of the disclination-induced strain hardening.

Let us introduce the quantity $\Delta = \tau_d/\tau_{d0}$, which denotes the ratio of the strain hardening in the presence of GB diffusion to strain hardening in its absence. Δ quantitatively characterizes the suppressing effect of diffusion on strain hardening. When the effect is small, Δ is close to 1. When diffusion significantly suppresses strain hardening, Δ is small (e.g. $\Delta \leqslant 0.5$ when diffusion decreases strain hardening by a factor of 2 or larger). Using Eqs. (3) and (8) and the relation $R = \kappa d$, Δ can be rewritten as

$$\Delta = 1 - \frac{f(s) - sf'(s)}{\ln(\kappa\alpha/\varepsilon) + 1}. \quad (9)$$

The dependences $\Delta(s)$, for $\kappa = 3, \alpha = 1/3$ and different values of ε, are shown in Fig. 4. As it follows from Fig. 4, Δ decreases with an increase in s and is considerably smaller than unity only at $s \gg 1$. This means that diffusion has a pronounced effect on the flow stress only in the region $s \gg 1$. In this region, using Eq. (6) and the relation $s = \lambda/(\gamma p^2) = \lambda\alpha^3/(\dot{\varepsilon}\varepsilon^2 d^3)$, Eq. (8) for τ_d can be simplified as

$$\tau_d|_{s \gtrsim 1} \approx \frac{A\omega^2\varepsilon}{\alpha}\left[\ln\frac{\kappa d}{(\lambda\varepsilon/\dot{\varepsilon})^{1/3}} + 0.25\right]. \quad (10)$$

According to Eq. (10), in the situation where GB diffusion is intensive, τ_d decreases with a decrease in the grain size d and/or strain rate $\dot{\varepsilon}$.

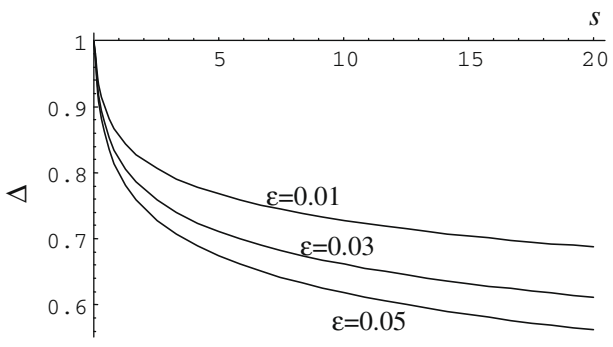

Fig. 4. Dependences of the parameter Δ (which characterizes the ratio of the strain hardening in the presence of GB diffusion to the strain hardening in its absence) on s for $\alpha = 1/3$ and $\kappa = 3$.

Now let us estimate the suppressing effect of diffusion on strain hardening in the cases of nanocrystalline Ni, Cu and Al_2O_3. We will use the Arrhenius relation (e.g. [61]) $D_b = D_{b0}\exp[-Q_b/(RT)]$, where $R = 8.31\ \mathrm{J\,K^{-1}}$ is the universal gas constant, Q_b is the GB self-diffusion activation energy, and D_{b0} is the pre-exponential factor. For nanocrystalline Ni, we have: $\Omega = 1.094 \times 10^{-29}\ \mathrm{m^3}$ [53], $D_{b0} = 1.8 \times 10^{-12}\ \mathrm{m^2\,c^{-1}}$ and $Q_b = 46\ \mathrm{k\,J\,mol^{-1}}$ [62]. For nanocrystalline Cu, we have: $\Omega = 1.181 \times 10^{-29}\ \mathrm{m^3}$ [53], $D_{b0} = 2.7 \times 10^{-9}\ \mathrm{m^2\,c^{-1}}$ and $Q_b = 61.8\ \mathrm{k\,J\,mol^{-1}}$ [62]. For nanocrystalline Al_2O_3, we used the values $D_{b0}\delta_b = 10^{-9}\ \mathrm{m^3\,c^{-1}}$ and $Q_b = 400\ \mathrm{k\,J\,mol^{-1}}$ [60]. In the case of Al_2O_3, the atomic volumes of Al and O atoms are different. Therefore, the value of Ω for Al_2O_3 can be interpreted as the average volume of Al_2O_3 per atom and is calculated as: $\Omega_{Al_2O_3} = \mu/(5\rho N_A)$, where $\mu = 0.102\ \mathrm{kg\,mol^{-1}}$ is the molar mass of Al_2O_3, $N_A = 6.02 \times 10^{23}\ \mathrm{mol^{-1}}$ is the Avogadro number, and $\rho \approx 3.9 \times 10^3\ \mathrm{kg\,m^{-3}}$ is the density of Al_2O_3 [54]. This yields: $\Omega_{Al_2O_3} = 0.87 \times 10^{-29}$. We also put $\delta_b = 0.5$ nm, $\kappa = 3$ and $\alpha = 1/3$.

The dependences of Δ on temperature T, for nanocrystalline Ni, Cu and $\alpha - Al_2O_3$, are presented in Fig. 5a, b and c, respectively, for $\varepsilon = 0.05$ and different values of d and $\dot{\varepsilon}$. It can be seen in Fig. 5 that Δ decreases with an increase in temperature T and/or decrease of grain size d and strain rate $\dot{\varepsilon}$. Thus, the suppressing effect of diffusion on disclination-induced strain hardening becomes more pronounced for smaller grain size d and/or smaller strain rate $\dot{\varepsilon}$. For nanocrystalline Ni and Cu, this effect becomes significant (making τ_d several times smaller) already at room temperature. For $\alpha - Al_2O_3$, the effect becomes significant at the temperatures around 1000–1200 K, depending on the grain size d and strain rate $\dot{\varepsilon}$.

It also follows from Fig. 5 that, for Cu and Ni at or near room temperature, the suppressing effect of diffusion on strain hardening is significant (Δ is around 0.5 or smaller) only for low strain rates ($10^{-4}\ \mathrm{s^{-1}}$ or smaller). Such small strain rates are most likely to happen during creep tests. At the same time, when temperature increases up to 330–360 K, the suppressing effect of diffusion on strain hardening becomes pronounced (Δ tends to have values of around 0.6–0.8) at intermediate strain rates of around $10^{-2}\ \mathrm{s^{-1}}$.

Fig. 6 plots the stress–strain curves $\tau_d(\varepsilon)$, for $T = 300$ K, $d = 10$ nm and different strain rates $\dot{\varepsilon}$. The dashed curves on the left depict the dependences $\tau_d(\varepsilon)$ in the absence of diffusion (at $\dot{\varepsilon} \to \infty$). It is seen from Fig. 6 that the suppressing effect of diffusion on strain hardening enhances with a decrease in strain rate $\dot{\varepsilon}$ and/or increase in plastic strain ε. Thus, Fig. 6 clearly demonstrates that sufficiently fast diffusion (occurring at a small enough strain rate or high enough temperature) can significantly diminish strain hardening.

Now let us calculate the strain rate sensitivity of NCMs plastically deformed by GB sliding accompanied by disclination formation and GB diffusion. The strain rate sensitivity is defined as (e.g. [32]) $m = (\dot{\varepsilon}/\sigma_t)\partial\sigma_t/\partial\dot{\varepsilon}$, where σ_t is

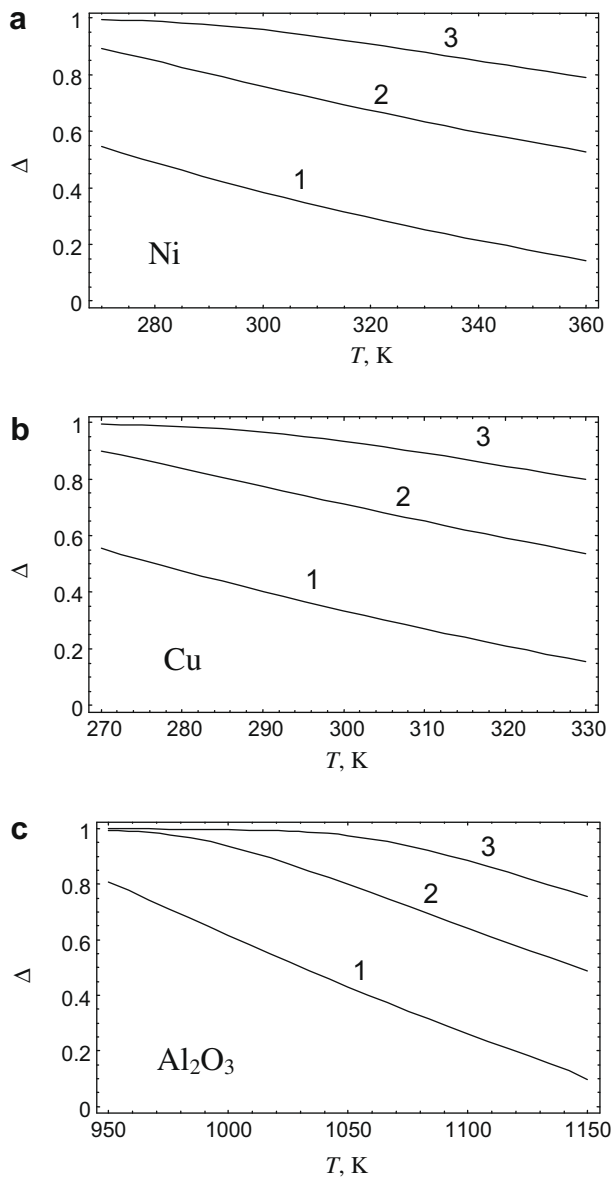

Fig. 5. Parameter Δ (which characterizes the ratio of the strain hardening in the presence of GB diffusion to the strain hardening in its absence) as a function of absolute temperature T, for nanocrystalline Ni (a), Cu (b) and Al_2O_3 (c), at $\alpha = 1/3, \kappa = 3, \varepsilon = 0.05; d = 10$ nm and $\dot{\varepsilon} = 10^{-4}$ s^{-1} (curves 1), $d = 10$ nm and $\dot{\varepsilon} = 10^{-2}$ s^{-1} (curves 2), and $d = 30$ nm and $\dot{\varepsilon} = 10^{-2}$ s^{-1} (curves 3).

the uniaxial load. The stress σ_t is calculated using Eq. (8) and the relation $\sigma_t = \sigma_y + 2\tau_d$.

Fig. 7a and b plot the strain rate sensitivities m as functions of strain rate $\dot{\varepsilon}$ and strain ε, respectively, for the case of nanocrystalline Ni at various grain sizes $d, T = 373$ K, $\sigma_y = 0.5$ GPa,$\alpha = 1/3, \kappa = 3, \omega = \pi/9$, and the values of the other parameters (elastic moduli and diffusion coefficient) specified above. Fig. 7 demonstrates that the values of m can vary over a wide range. At the same time, m tends to increase with a decrease in $\dot{\varepsilon}$. Physically, this tendency is associated with the fact that, for high strain rates, diffusion is too slow to exert a significant influence on the flow stress. In this case, the flow stress is controlled by the disclination-induced strain hardening. At the same time, at small strain rates, diffusion contributes considerably to the plastic deformation and flow stress, and this contribution results in a high strain rate sensitivity. As follows from Fig. 7, strain rate sensitivity m also grows with a decrease in grain size d. At the same time, the dependence of strain rate sensitivity m on strain ε is not monotonous: m first increases and then decreases with rising ε. (The region at curve 3 where m decreases with rising ε is not shown in Fig. 7b).

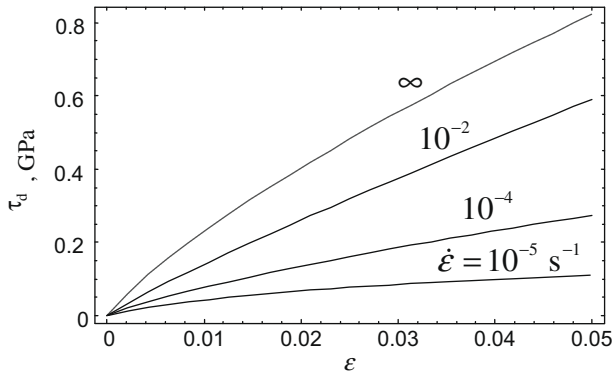

Fig. 6. Dependences of stress τ_d on plastic strain ε for Cu, at $\kappa = 3$, $\alpha = 1/3, \omega = \pi/9, d = 10$ nm, $T = 300$ K, and different strain rates $\dot{\varepsilon}$.

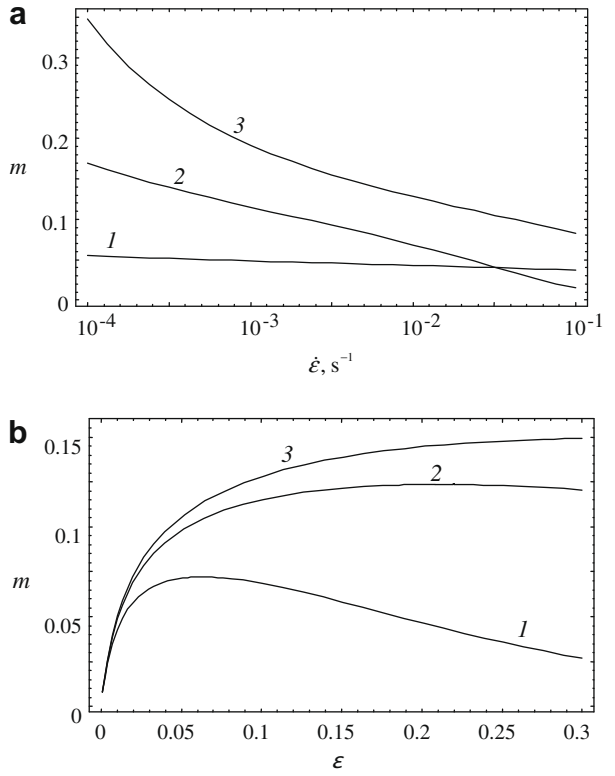

Fig. 7. Dependences of strain rate sensitivity m of deformed nanocrystalline Ni on strain rate $\dot{\varepsilon}$ (a) and strain ε (b) at $\kappa = 3, \alpha = 1/3, \omega = \pi/9, T = 373$ K. (a) $\varepsilon = 0.01, d = 40$ nm (curve 1); $\varepsilon = 0.1, d = 40$ nm (curve 2); $\varepsilon = 0.1, d = 15$ nm (curve 3). (b) $\dot{\varepsilon} = 10^{-2}$ s$^{-1}, d = 40$ nm (curve 1); $\dot{\varepsilon} = 10^{-3}$ s$^{-1}, d = 40$ nm (curve 2); $\dot{\varepsilon} = 10^{-2}$ s$^{-1}, d = 15$ nm (curve 3).

Low values of m at small ε are associated with the absence of disclination dipoles (the driving force for diffusion) at the initial stage of plastic deformation. As a result, for small ε, the rate of disclination-induced diffusion is slow, and diffusion cannot contribute greatly to the plastic flow. As ε grows, the driving force for diffusion appears, and strain rate sensitivity increases. At the same time, with a further increase in ε, the flow stress becomes so large that diffusion cannot significantly reduce it. As a corollary, the strain rate sensitivity m reduces.

Fig. 7 plots the dependences of m on $\dot{\varepsilon}$ and ε in the situation where the dominant deformation mechanism is the diffusion-accommodated GB sliding. It should be noted, however, that in situations where several deformation mechanisms act simultaneously, the strain dependence of m can have a different character. For example, in the situation where the Coble creep significantly contributes to plastic deformation at small enough strain rates, the existence of this deformation mode provides high values of m even at small ε. Also, when the grain size of a nanocrystalline specimen is large enough, dislocation slip can gradually be activated in various grains as the flow stress increases. In this case, with increasing plastic strain (and, consequently, flow stress), the fraction of grains where dislocation slip occurs also increases, and the contribution of dislocation slip to the overall plastic deformation rises. As a consequence, in this situation, strain rate sensitivity m can also fall down with an increase in strain even at small ε.

Now let us compare the calculated values of m with the experimental data [42] for the strain rate sensitivity of uniaxially compressed nanocrystalline Ni with grain size $d = 40$ nm at the temperature $T = 373$ K, when strain rate ranges from approximately 10^{-7} to 10^{-3} s^{-1}. The experimental points in Fig. 4a in Ref. [42] demonstrate that m is either independent of strain rate $\dot{\varepsilon}$ or very weakly decreases with an increase in $\dot{\varepsilon}$. The experimental dependence $m(\dot{\varepsilon})$ documented in Ref. [42] is qualitatively similar to the theoretical dependence shown in curve 1 in Fig. 7a here. At the same time, the experimental measurements of the dependence of $m(\varepsilon)$ in Ref. [42] demonstrate a decrease in m from approximately 0.125 to approximately 0.08 with an increase in ε from 0.01 to 0.04. (An increase in ε is accompanied by a decrease in $\dot{\varepsilon}$ [42], but the latter fact can be neglected due to a very weak $m(\dot{\varepsilon})$ dependence documented in Ref. [42].) The experimental dependence of $m(\varepsilon)$ differs from the calculated dependences shown in Fig. 7b. This can be explained by the co-operative actions of various deformation mechanisms in nanocrystalline specimens examined experimentally [42] (see above).

5. Ductility maps of nanocrystalline materials

In parallel with diminishing strain hardening, intensive diffusion suppresses crack generation and growth. At the same time, to achieve a good plastic behavior, diffusion should not be too fast. This is necessary to provide strain hardening sufficient to suppress the plastic strain instability leading to necking. Thus, for a specified strain rate, the rate of diffusion should be in an optimum range. That is, the rate of diffusion should be high enough to decrease strain hardening and suppress crack generation and growth but, at the same time, small enough to suppress plastic strain instability. The rate of diffusion can be controlled by tuning grain size and temperature.

Based on the analysis of the previous sections, let us first roughly estimate the material and deformation parameters (that determine the rate of diffusion) at which an NCM is stable to necking. As above, we will focus on the NCMs with the finest grains, in which GB sliding serves as the dominant deformation mechanism. Following Hart [63], a solid under a uniaxial tensile load σ_t, deformed with a strain rate $\dot{\varepsilon}$ up to a strain ε, is stable with respect to necking if

$$\frac{1}{\sigma_t}\frac{\partial \sigma_t}{\partial \varepsilon} + m \geqslant 1. \tag{11}$$

The left-hand side of Eq. (11) defines the normalized effective strain hardening. The solution of inequality (11) gives the set of parameters at which a deformed solid is stable to necking. In the case where diffusion rate is not negligible and, at the same time, not too fast (i.e. the parameter Δ lies in the range of about 0.1–0.95), we can calculate σ_t using Eq. (10) combined with the relation $\sigma_t = \sigma_y + 2\tau_d$. Then, after substitution of both Eq. (10) and the latter relation to Eq. (11), with the assumption that $\varepsilon \ll 1$, Eq. (11) is rewritten in the following form:

$$\dot{\varepsilon} \geqslant \frac{\lambda \varepsilon}{\kappa^3 d^3} \exp\left(\frac{3\alpha\sigma_y}{2A\omega^2} + 0.24\right). \tag{12}$$

In Eq. (12) the quantity λ depends on temperature T due to the temperature dependence of the GB diffusion coefficient D_b.

Now let us consider the respective contributions of the strain rate sensitive and insensitive parts of the normalized effective strain hardening given by the left-hand side of Eq. (11). To do so, we rewrite Eq. (11) as follows:

$$h_0 + h_{dif} + m \geqslant 1. \tag{13}$$

Here the strain rate insensitive part is given as $h_0 = (1/\sigma_{t0})\partial\sigma_{t0}/\partial\varepsilon$, where $\sigma_{t0} = \sigma_y + 2\tau_{d0}$ is the tensile stress in the absence of GB diffusion. h_0 is always positive, because it is related to the strain hardening created by disclination dipoles. The strain rate sensitive part consists of the two terms, h_{dif} and m, shown in Eq. (13). The second term—strain rate sensitivity m—is always positive. The former term h_{dif} is associated with the effect of diffusion on the strain hardening, i.e. $h_{dif} = (1/\sigma_t)(\partial\sigma_t/\partial\varepsilon) - (1/\sigma_{t0})\partial\sigma_{t0}/\partial\varepsilon$. Since GB diffusion decreases stress σ_t at a specified strain ε and, as a corollary, reduces the strain hardening, h_{dif} is always negative. Our estimates show that h_{dif} is larger by an order of magnitude than m, and so the strain rate sensitive part $(h_{dif} + m)$ of the normalized effective strain hardening is negative. In addition, our estimates show that the strain rate sensitive part $h_{dif} + m$ can considerably

reduce the normalized effective strain hardening if the strain rate is small enough and diffusion is sufficiently fast (so that the value of Δ is considerably smaller than unity; see Fig. 5). For example, for nanocrystalline Cu with $d = 10$ nm at $T = 330$ K and $\varepsilon = 0.05$, for $\dot{\varepsilon} = 10^{-4}$ s^{-1} (corresponding to $\Delta \approx 0.15$; see Fig. 5b), we obtain $h_0 = 11.5$ and $h_{dif} + m = -8.2$, respectively. At the same time, for $\dot{\varepsilon} = 10^{-2}$ s^{-1} (corresponding to $\Delta \approx 0.6$; see Fig. 5b), the calculated values of the strain rate insensitive and sensitive parts of the normalized effective strain hardening are $h_0 = 11.5$ and $h_{dif} + m = -0.6$. In doing so, the total normalized effective strain hardening $h_0 + h_{dif} + m$, for $\dot{\varepsilon} = 10^{-4}$ s^{-1} and $\dot{\varepsilon} = 10^{-2}$ s^{-1}, is equal to 3.3 and 10.9, respectively. This illustrates the tendency that increasing strain rate will result in higher strain hardening. At the same time, GB diffusion decreases the normalized effective strain hardening, in which case decreasing strain rate will result in lower strain hardening. In particular, GB diffusion can decrease the normalized effective strain hardening up to the level at which a nanocrystalline specimen is unstable to necking. For instance, in the situation of nanocrystalline Cu with $d = 10$ nm, $T = 330$ K and $\varepsilon = 0.1$, for $\dot{\varepsilon} = 10^{-4}$ s^{-1} (corresponding to $\Delta \approx 0.11$), the values of the strain rate insensitive and sensitive parts are $h_0 = 5.89$ and $h_{dif} + m = -5.04$, respectively. In this situation, the total normalized effective strain hardening $h_0 + h_{dif} + m$ is equal to 0.85, and, following the Hart criterion (13), plastic strain instability occurs.

Thus, sufficiently fast diffusion can significantly diminish strain hardening, thereby making a nanocrystalline specimen unstable to necking. At the same time, if diffusion is too slow, the flow stress may become very high, in which case a nanocrystalline specimen can fracture through the formation and growth of cracks. A microscopic analysis of the formation and growth of cracks in NCMs deformed through GB sliding and diffusion and the calculation of the deformation parameters at which such NCMs fractures is a very complicated problem that is beyond the scope of this paper. To make a rough estimate of the deformation parameters (strain ε, strain rate $\dot{\varepsilon}$ and temperature T) at which an NCM begins to fracture due to catastrophic growth of cracks, we will use a simple first-approximation phenomenological approach. We assume that an NCM is stable to fracture if the flow stress is smaller than some critical value σ_B ($\sigma_\pm < \sigma_B$), where σ_B can be interpreted as the ultimate tensile strength of such an NCM.

The criterion $\sigma_\pm < \sigma_B$ allows one to estimate the deformation parameters at which an NCM can fracture. To do so, we insert this criterion into both Eq. (10) and the relation $\sigma_t = \sigma_y + 2\tau_d$. This yields the following condition for the stability of an NCM with respect to catastrophic cracking:

$$\dot{\varepsilon} < \frac{\lambda\varepsilon}{\kappa^3 d^3} \exp\left(\frac{3\alpha(\sigma_B - \sigma_y)}{2A\omega^2\varepsilon} - 0.75\right). \tag{14}$$

Now let us focus on the exemplar case of nanocrystalline Cu with the grain size $d = 15$ nm. We set $\omega = 20°$ and employ the material parameters for nanocrystalline Cu specified in Sections 3 and 4. Also, for simplicity, we assume that its yield strength σ_y is independent of temperature and equal to 0.5 GPa (the value for Cu with the grain size 15 nm obtained in Ref. [64]). For definiteness, we also put $\sigma_B = 1$ GPa.

Fig. 8 plots the ductility maps for nanocrystalline Cu in the coordinates $(T, \dot{\varepsilon})$ for $\varepsilon = 0.05$ (Fig. 8a) and $\varepsilon = 0.1$ (Fig. 8b). The curves in Fig. 8 separate the parameter regions where nanocrystalline Cu is stable to failure at a given strain ε from the regions where it is unstable to failure through necking or fracture. As can be seen in Fig. 8, nanocrystalline Cu can demonstrate good ductility over a certain range of strain rates $\dot{\varepsilon}$ and temperatures T. With an increase in strain ε, the middle parameter region in the maps (where Cu exhibits good ductility) shrinks (see Fig. 8a and b), and this region completely disappears at some critical strain ε_c. The critical strain ε_c can be calculated by equating the right-hand sides of Eqs. (12) and (14) as

$$\varepsilon_c = \frac{3\alpha(\sigma_B - \sigma_y)}{3\alpha\sigma_y + 2A\omega^2}. \tag{15}$$

Note that ε_c does not depend on T. As a corollary, the two curves on the ductility map (see Fig. 8) become identical at $\varepsilon = \varepsilon_c$. For nanocrystalline Cu with the parameter values specified above, we find: $\varepsilon_c \approx 0.15$.

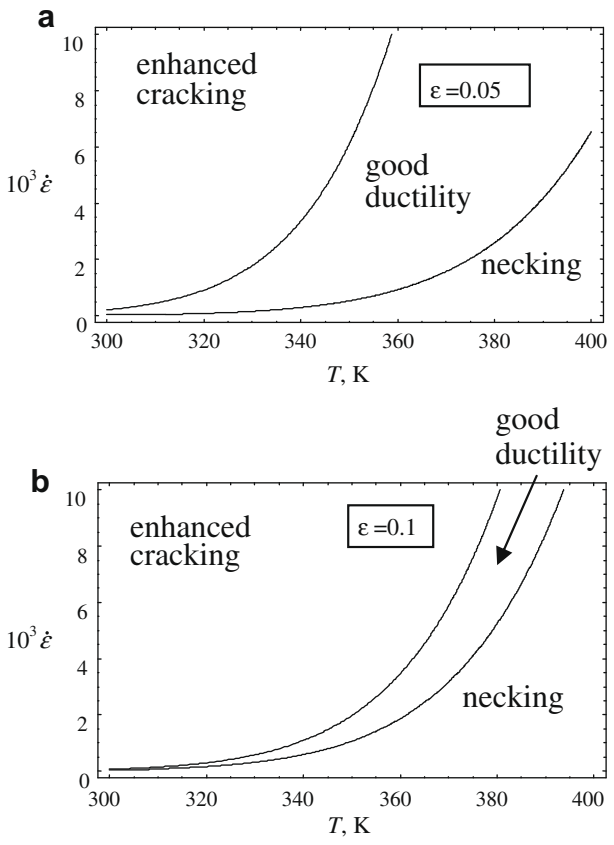

Fig. 8. Ductility maps of nanocrystalline Cu with the grain size $d = 15$ nm in the coordinates $(T, \dot{\varepsilon})$, for $\varepsilon = 0.05$ (a) and $\varepsilon = 0.1$ (b).

It should also be noted that the maps in Fig. 8 are very approximate due to the strong model approximations, approximations in the calculations and uncertainties in the values of some parameters (e.g. $\omega, \sigma_y, \sigma_B, D_b$), which depend on the fabrication procedure and initial structure of an NCM. However, these maps demonstrate that there is a range of deformation parameters in which NCMs can be stable to failure. As plastic deformation proceeds, this range shrinks, and at some critical strain ε_c the NCM starts to fail at any deformation rate $\dot{\varepsilon}$ and temperature T.

6. Conclusions

Following the results of the theoretical analysis given in this paper, GB sliding in nanocrystalline metals and ceramics produces wedge disclinations that cause competing effects on the ductility of NCMs. First, the formation of disclinations provides dramatic strain hardening (which suppresses plastic strain instability) in deformed NCMs and thereby enhances their ductility. At the same time, dramatic strain hardening induced by disclinations results in large flow stresses, which can initiate the enhanced formation and/or growth of cracks [29] and eventually result in the complete fracture of the material. Intensive GB diffusion can release disclination stresses, thereby reducing strain hardening and suppressing crack nucleation and growth. For a specified strain rate, the rate of diffusion should be high enough to decrease strain hardening and suppress crack generation but, at the same time, small enough to suppress plastic strain instability. At the same time, for a specified strain, there exists an interval of strain rates and temperatures at which an NCM is stable to necking and catastrophic fracture. With an increase in strain this interval shrinks, and at some critical strain it disappears. Above this critical strain, an NCM can no longer be stabilized with respect to failure by either necking or fracture through the optimization of its deformation regime.

The results of our model are in agreement with several experimental findings on the deformation behavior of NCMs. In particular, there are examples of good tensile ductility exhibited by nanomaterials at room temperature and low loading rates. For instance, Champion et al. [10] reported on strain-to-failure of nanocrystalline Cu equal to 14% at the low strain rate of 5×10^{-6} s^{-1}. Li and Ebrahimi [55,65] experimentally observed good ductility (characterized by the strain-to-failure of 8–9%) of nanocrystalline Ni and Ni–15% Fe at the strain rate of 10^{-4} s^{-1}. Also, there are experimental data showing an increase in strain-to-failure of nanomaterials with a decrease in strain rate. For instance, Karimpoor et al. [33] experimentally documented both good tensile ductility of nanocrystalline Co at room temperature and a substantial increase in strain-to-failure (from 6% to 9%) with a decrease in strain rate from 2.5×10^{-3} to 10^{-4} s^{-1}. The above experimental observation directly demonstrates that, if the loading rate gets very slow, one can achieve significantly higher ductility at room temperature.

Finally, note that, in parallel with GB sliding, other plastic deformation mechanisms can also operate in NCMs. These deformation mechanisms—lattice slip (carried by dislocations emitted from GBs), twin deformation, Coble creep, rotational deformation [1–7]—influence the ductility of NCMs. At the same time, our model describing the role of GB sliding and diffusion processes in the tensile ductility of nanocrystalline metals and ceramics captures the essential physics of plastic flow in NCMs under certain conditions where GB sliding serves as the dominant deformation mechanism.

Acknowledgments

The work was supported, in part, by the Russian Foundation of Basic Research (grant 08-01-00225-a), the Office of Naval Research (grant N00014-08-1-0405), the National Science Foundation (grant CMMI #0700272), the Russian Federal Agency of Science and Innovations (grant MK-1702.2008.1), and the Russian Academy of Sciences Program "Basis of fundamental studies in nanotechnologies and nanomaterials".

Appendix

In this Appendix, we calculate the self-energy of an expanding disclination dipole at an infinite straight GB in the presence of GB diffusion (Fig. 2b). To do so, we designate the stress field of a disclination dipole in the GB region as $\sigma_{jk}(x,t)$ and the elastic displacements between the borderline between the GB region and the upper grain interior as $u_j(x,t)$. Let $\delta(x,t)$ be a change in the GB thickness due to the presence of the disclination dipole and GB diffusion induced by the disclination stresses (Fig. 2b). The quantity $\delta(x,t)$ is also equal to the jump of displacements $u_y(x,y,t)$ (created by the disclination dipole and GB diffusion) at the GB. The displacements $u_y(x,y,t)$ created by the disclination dipole are symmetric about the GB plane $y = 0$. Therefore, the elastic displacement $u_y(x,t)$ of the borderline between the GB region and the upper grain interior is equal to $\delta/2$ (Fig. 2b).

The strain energy W^{dip} of the disclination dipole (per unit disclination length) in the presence of GB diffusion can be written as [66]

$$W^{dip} = -\frac{1}{2}\int_{-R}^{R} \sigma_{yy}(x,t)\delta(x,t)dx, \tag{A1}$$

where R is the screening length of the stresses created by the disclination dipole. We have: $\delta(x,t) = 2u_y(x,t)$. In this case, in order to calculate the strain energy W^{dip}, we need to compute the stresses $\sigma_{yy}(x,t)$ and displacements $u_y(x,t)$ created by the disclination dipole.

To do so, in the following, we will use the results of the approach given in Refs. [25,60], which allow one to calculate the stresses induced by stress sources in the GB by solving a linearized diffusion equation combined with the equations of linear elasticity. In this linear approach, the

elastic fields created by several stress sources appear to be the sums of the corresponding elastic fields induced by individual stress sources. However, the linearized diffusion equation used in this approach is accurate under the condition $\sigma\Omega/(k_BT) \ll 1$, where $\sigma = 1/3(\sigma_{xx} + \sigma_{yy} + \sigma_{zz}), \sigma_{xx}, \sigma_{yy}$ and σ_{zz} are the stresses acting in the GB, Ω is the atomic volume, k_B is the Boltzmann constant, and T the absolute temperature. At and near the disclination cores of disclination dipoles originating due to GB sliding, the above relation is not satisfied. Comparing one-dimensional diffusion equation and its linearized form [25,60,67], one can assume that this results in an underestimate of the diffusion rate and an overestimate of the temperature required to provide an essential diffusion effect on GB sliding. This overestimate of the temperature is the higher, the larger the disclination strength ω and dipole arm p. However, even for large ω and p, the use of the linearized diffusion equation [25,60] reveals the semi-quantitative tendencies associated with the influence of GB diffusion on strain hardening.

To calculate $\sigma_{yy}(x,t)$ and $u_y(x,t)$, we present the disclination dipole as a continuous uniform distribution of virtual edge dislocations (with the infinitesimal Burgers vectors $d\mathbf{B} = -\omega\, dx\, \mathbf{e}_y$) in the interval $0 \leqslant x \leqslant p$ (see Fig. 2b). Further, we suppose that the material examined is deformed with a constant shear strain rate $\dot{\varepsilon}$, which yields: $p = \gamma t = (\dot{\varepsilon} d/\alpha)\, t$. This means that at the time point $t = t'$ the right (moving) disclination lies at the point $x = x' = \gamma t'$, while at the time instance $t' + dt'$ it moves to the point $x = x' + dx' = x' + \gamma\, dt'$. This is equivalent to the appearance of a new virtual dislocation (at the point $x = x'$ and time instance $t = t'$) with the infinitesimal Burgers vector $d\mathbf{B} = -\omega\, dx'\, \mathbf{e}_y = -\omega\gamma\, dt'\, \mathbf{e}_y$. Therefore, due to the linearity of the problem (see above), the stress $\sigma_{yy}(x,t)$ (displacement $u_y(x,t)$, respectively) can be written as the superposition of the corresponding stresses (displacements, respectively) created by the virtual dislocations with the above Burgers vectors:

$$\sigma_{yy}(x,t) = \omega\gamma \int_0^t \sigma^d_{yy}(x - \gamma t', t - t')\, dt', \tag{A2}$$

$$u_y(x,t) = \omega\gamma \int_0^t u^d_y(x - \gamma t', t - t')\, dt'. \tag{A3}$$

Here $\sigma^d_{yy}(x,t)$ and $u_y(x,t)$ are the stress and displacement, respectively, created at the borderline between the GB and the upper grain interior by the dislocation with the unit Burgers vector $\mathbf{B} = -\mathbf{e}_y$, originating at the point $x = 0$ of the GB at the time instance $t = 0$.

The stress $\sigma^d_{yy}(x,t)$ and displacement $u^d_y(x,t)$ can be presented [25] as

$$\sigma^d_{yy}(x,t) = \frac{iA}{2} \int_{-\infty}^{\infty} \operatorname{sign} k\, \exp(-\lambda|k^3|t)\, \exp(ikx)\, dk, \tag{A4}$$

$$u^d_y(x,t) = -\frac{1-\nu}{2G}\, iA \int_{-\infty}^{\infty} \frac{\exp(-\lambda|k^3|t)\, \exp(ikx)}{k}\, dk, \tag{A5}$$

where $i = \sqrt{-1}, \lambda = (1+\nu)\, GD_b\delta_b\, \Omega/[3(1-\nu)\, k_BT]$, and D_b denotes the GB diffusion coefficient.

Insertion of (A4) into (A2) and (A5) into (A3) yields:

$$\sigma_{yy}(x,t) = \frac{iA\omega\gamma}{2} \int_{-\infty}^{\infty} \frac{\exp(-ik\gamma t) - \exp(-\lambda|k^3|t)}{\lambda|k^3| - ik\gamma} \operatorname{sign} k\, \exp(ikx)\, dk, \tag{A6}$$

$$u_y(x,t) = -\frac{i\omega\gamma}{4\pi} \int_{-\infty}^{\infty} \frac{\exp(-ik\gamma t) - \exp(-\lambda|k^3|t)}{k(\lambda|k^3| - ik\gamma)} \exp(ikx)\, dk. \tag{A7}$$

Now the energy W^{dip} is calculated by the substitution of (A6) and (A7) to (A1). After calculations, we obtain:

$$W^{dip}(R \gg (p, (\lambda t)^{1/3})) = \frac{A\omega^2 p^2}{2} \left[\ln\frac{R}{p} + \frac{3}{2} - f(s)\right], \tag{A8}$$

where $s = \lambda/(\gamma p^2) = \lambda t/p^3$ is the cube of the ratio of the characteristic diffusion length $(\lambda t)^{1/3}$ to the dipole arm p, and

$$f(u) = \int_0^{\infty} \left(\frac{2(1-\cos k)}{k^3} - \frac{1 - 2\cos k\, \exp(-uk^3) + \exp(-2uk^3)}{k^3(u^2k^4 + 1)}\right) dk. \tag{A9}$$

References

[1] Kumar KS, Suresh S, Van Swygenhoven H. Acta Mater 2003;51:5743.
[2] Wolf D, Yamakov V, Phillpot SR, Mukherjee AK, Gleiter H. Acta Mater 2005;53:1.
[3] Han BQ, Lavernia E, Mohamed FA. Rev Adv Mater Sci 2005;9:1.
[4] Ovid'ko IA. Int Mater Rev 2005;50:65.
[5] Meyers MA, Mishra A, Benson DJ. Prog Mater Sci 2006;51:427.
[6] Dao M, Lu L, Asaro RJ, De Hosson JTM, Ma E. Acta Mater 2007;55:4041.
[7] Koch C, Ovid'ko IA, Seal S, Veprek S. Structural nanocrystalline materials: fundamentals and applications. Cambridge: Cambridge University Press; 2007.
[8] Mukherjee AK. Mater Sci Eng A 2002;322:1.
[9] Sergueeva AV, Mukherjee AK. Rev Adv Mater Sci 2006;13:1.
[10] Champion Y, Langlois C, Guerin-Mailly S, Langlois F, Bonnentien J-L, Hytch M. Science 2003;300:310.
[11] Youssef K-M, Scattergood RO, Murty KL, Koch CC. Appl Phys Lett 2004;85:929; Scripta Mater 2006;54:251.
[12] Youssef KM, Scattergood RO, Murty KL, Horton JA, Koch CC. Appl Phys Lett 2005;87:091904.
[13] Sergueeva AV, Mara NA, Krasilnikov NA, Valiev RZ, Mukherjee AK. Philos Mag 2006;86:5797.
[14] Valiev RZ. Nat Mater 2004;3:511.
[15] Xu X, Nishimura T, Hirosaki N, Xie RJ, Yamamoto Y, Tanaka H. Acta Mater 2006;54:255.
[16] Weissmüller J, Markmann J. Adv Eng Mater 2005;7:202.
[17] Van Swygenhoven H, Derlet PA. Phys Rev B 2001;64:22.
[18] Farkas D, Curtin WA. Mater Sci Eng A 2005;412:316.
[19] Monk J, Hyde B, Farkas D. J Mater Sci 2006;41:7741.
[20] Van Swygenhoven H, Spaczer M, Caro A. Acta Mater 1999;47:561.
[21] Wei Y, Bower AF, Gao H. Acta Mater 2008;56:1741.
[22] Padmanabhan KA, Gleiter H. Mater Sci Eng A 2004;381:28.
[23] Ovid'ko IA, Sheinerman AG. Acta Mater 2004;52:1209.
[24] Gutkin MYu, Ovid'ko IA, Skiba NV. Acta Mater 2004;52:1711.
[25] Ovid'ko IA, Sheinerman AG. Acta Mater 2005;53:1347.
[26] Pande CS, Masumura RA. Mater Sci Eng A 2005;409:125.
[27] Mohamed FA, Chauhan M. Metall Mater Trans A 2006;37:3555.
[28] Mohamed FA. Metall Mater Trans A 2007;38:340.
[29] Ovid'ko IA, Sheinerman AG. Appl Phys Lett 2007;90:171927.
[30] Koch CC. Scripta Mater 2003;49:657.
[31] Ma E. Scripta Mater 2003;49:663.

[32] Wang YM, Ma E. Acta Mater 2004;52:1699.
[33] Karimpoor AA, Erb U, Aust KT, Palumbo G. Scripta Mater 2003;49:651.
[34] Kumar KS, Suresh S, Chisholm MF, Norton JA, Wang P. Acta Mater 2003;51:387.
[35] Zhan G-D, Kuntz JD, Wan J, Mukherjee AK. MRS Bull 2004;29:22.
[36] Ovid'ko IA, Sheinerman AG. Phys Rev B 2008;77:054109.
[37] Ovid'ko IA, Sheinerman AG, Aifantis EC. Acta Mater 2008;56:2718.
[38] Kaibyshev OA. Superplasticity of industrial alloys. Moscow: Metallurgiya; 1984 [in Russian].
[39] Langdon TG. J Mater Sci 2006;41:597.
[40] Mayo MJ, Siegel RW, Narayanasamy A, Nix WD. J Mater Res 1990;5:1073.
[41] Mayo MJ, Siegel RW, Liao YX, Nix WD. J Mater Res 1992;7:973.
[42] Kottada RS, Chokshi AH. Scripta Mater 2005;53:887.
[43] Cheng S, Ma E, Wang YM, Kecskes LJ, Youssef KM, Koch CC, et al. Acta Mater 2005;53:1521.
[44] Wang YM, Hamza AV, Ma E. Acta Mater 2006;54:2715.
[45] Jiang Z, Liu XL, Li GY, Jang Q, Lian JS. Appl Phys Lett 2006;88:143115.
[46] Lu L, Sui ML, Lu K. Science 2000;287:1463.
[47] Wang N, Wang Z, Aust KT, Erb U. Mater Sci Eng A 1997;237:150.
[48] Yin WM, Whang SH, Mishams R, Xiao CH. Mater Sci Eng A 2001;301:18.
[49] Wang GF, Chan KC, Zhang KF. Scripta Mater 2006;54:765.
[50] Zhou X, Hulbert DM, Kuntz JD, Sadangi RK, Shukla V, Kear BH, et al. Mater Sci Eng A 2005;394:353.
[51] Orowan E. Proc Phys Soc 1940;52:8.
[52] Romanov AE, Vladimirov VI. In: Nabarro FRN, editor. Dislocations in solids, vol. 9. Amsterdam: North-Holland; 1992. p. 191.
[53] Smithells CJ, Brands EA. Metals reference book. London: Butterworth; 1976.
[54] Munro RG. J Am Ceram Soc 1997;80:1919.
[55] Li H, Ebrahimi F. Appl Phys Lett 2004;84:4307.
[56] Gutkin MYu, Ovid'ko IA, Skiba NV. J Phys D 2005;38:3921.
[57] Fu H-H, Benson DJ, Meyers MA. Acta Mater 2001;49:2567.
[58] Gutkin MYu, Ovid'ko IA, Skiba NV. J Phys D 2003;36:L47.
[59] Ovid'ko IA, Sheinerman AG. Philos Mag 2007;87:4181.
[60] Evans AG, Rice JR, Hirth JP. J Am Ceram Soc 1980;63:368.
[61] Sutton AP, Balluffi RW. Interfaces in crystalline materials. Oxford: Clarendon Press; 1995.
[62] Kolobov YuR, Valiev RZ, Ivanov MB. Grain boundary diffusion and properties of nanostructured materials. Cambridge: Cambridge International Science Publishing; 2007.
[63] Hart EW. Acta Metall 1967;15:351.
[64] Chokshi AH, Rosen A, Karch J, Gleiter H. Scripta Metall 1989;23:1679.
[65] Li H, Ebrahimi F. Adv Mater 2005;17:1969.
[66] Mura T. In: Herman H, editor. Advances in materials research. New York: Interscience; 1968. p. 1–107.
[67] Raj R, Ashby MF. Metall Trans 1971;2:1113.